A STABLE COMPLEX-ANALYTIC FRAMEWORK FOR AIR-ATTENUATION AND DISPERSION CORRECTION IN ACOUSTIC SCALE MODELS

S Koyanagi, K Suzuki, Y Yamada, T Hidaka Takenaka R&D Institute, Chiba, Japan

1 INTRODUCTION

Scaled model experiments are a common and essential technique in architectural acoustics for predicting and evaluating acoustic characteristics of full-scale spaces[1]. This allows the study of complex wave phenomena, such as reflections, diffractions, and interferences, which computer simulations often cannot fully capture. Consequently, it allows the optimization of architectural designs to achieve the desired acoustic environments before actual construction.

The fundamental principle requires strict adherence to similarity laws. For a model scaled by 1/N, measurements must be conducted at frequencies N times higher than those of interest in a full-scale environment. However, this frequency scaling poses a considerable challenge, because the physical properties of air do not follow the same similarity laws. For the accurate auralization of the audible band (0–10 kHz) in a 1/10-scale model, the measurements must be extended to 100 kHz. However, at 100 kHz, air absorption dominates and produces attenuation far beyond the full-scale conditions.

Two main approaches address this issue: physical control of gas composition and numerical correction of measured impulse responses. Physical methods involve the use of dry air or nitrogen to reduce absorption; however, they require specialized equipment and still face practical limits above certain frequencies[1,2]. Numerical correction techniques, such as Polack's MIDAS package using the short-time Fourier transform[2] and digital filtering-based correction methods[3], have been effective in correcting air absorption, but they face challenges with increased background noise during the correction process[4]. Note that both numerical correction techniques have a finite time and/or frequency resolution.

With recent advances in spatial audio technologies, there is a growing demand for high-fidelity reproduction of sound fields such as ambisonics for scale models[5]. However, the 1/8 inch microphones often used in measurements have non-negligible dimensions relative to the model scale, making multichannel array microphones impractical. Instead, a single microphone must be moved to multiple positions. This process is time-consuming, and strict environmental control is required to minimize variations in temperature and humidity during measurements. Accurate correction of dispersion and phase velocity would enable correction for subtle changes in air conditions during measurement, potentially leading to high-quality auralization.

To address these challenges, we developed a refined compensation framework. In our earlier work[6], we proposed a theoretical approach that treated the observed impulse response as a superposition of plane waves radiated from an unknown "virtual source distribution" along the propagation path. Once this distribution is determined, an impulse response for the desired air propagation constant can be synthesized, enabling compensation under various environmental conditions. However, direct numerical computation faces severe instabilities, particularly for long propagation times, requiring frequency-domain windowing, which limits numerical accuracy.

This study refines our analytical approach based on complex analysis[7] to develop a unified correction framework that addresses both absorption and dispersion. Our method avoids numerical singularities and arbitrary parameters while integrating scale conversion and environmental compensation into a single procedure. We demonstrate the complete theoretical framework and validate its practical performance using a 1/10-scale room model with combined corrections for scale conversion and temperature-humidity variation.

2 THEORY: ANALYTICAL CORRECTION METHOD

2.1 Formulation Using Virtual Source Distribution

The proposed correction method is based on the concept of virtual source distribution6. When sound reflects off room boundaries, each reflection can be modeled as originating from the mirror image of the source. Each reflected contribution travels from x_0 toward the measurement origin, and its amplitude is determined by the boundary reflections and attenuation in air. Arranging these hypothetical source strengths along the propagation coordinate x_0 defines the virtual source distribution $\phi(x_0)$.

Under the far-field (plane-wave) approximation, the measured impulse response is the superposition of these contributions. By treating each as a plane wave and integrating over all distances, the Fourier transform of the impulse response $\hat{h}(\omega)$ is given by the sum of the contributions of $\phi(x_0)$:

$$\hat{h}(\omega) = \frac{1}{2\pi}\int_{-\infty}^{0} e^{\gamma_h(\omega)x_0}\phi(x_0)\, dx_0 \tag{1}$$

where ω denotes angular frequency and $\gamma_h(\omega)$ the propagation constant of air. This equation indicates that $\hat{h}(\omega)$ represents the Laplace transform of $\phi(x_0)$. Therefore, $\phi(x_0)$ can be mathematically determined uniquely through inverse transformation

$$\phi(x_0) = i\int_{-\infty}^{\infty} \frac{d\gamma_h(\omega)}{d\omega}\hat{h}(\omega)e^{-\gamma_h(\omega)x_0}d\omega \tag{2}$$

The virtual source distribution $\phi(x_0)$ depends solely on the room geometry and materials of the room surfaces and is independent of the propagation medium. Once $\phi(x_0)$ is obtained, the impulse response can be synthesized in the target medium with an arbitrary propagation constant that differs from that of the experimental system.

In a $1/N$ scale model experiment, the measured impulse response is transformed to its full-scale equivalent for acoustic analysis and auralization. This transformation expands the virtual source distribution by a factor of N, mapping $\phi(x_0) \longmapsto \phi(x_0/N)/N$. Substituting this transformation into Equation (2), the scale transformation is equivalent to

$$\gamma_h(\omega) \longmapsto \gamma_h(\omega)/N \tag{3}$$

Thus, according to Equation (3), the scale transformation in the model experiments can be implemented by modifying the propagation constant,. By eliminating $\phi(x_0)$, an integral transformation equation can be derived from the measured response $\hat{h}(\nu)$ to the corrected response $\hat{r}(\omega)$

$$\hat{r}(\omega) = \frac{i}{2\pi}\int_{-\infty}^{\infty} \frac{d\gamma_h(\nu)}{d\nu}\hat{h}(\nu)\left(\int_{-\infty}^{0} e^{(-\gamma_h(\nu)+\gamma_r(\omega))x_0}\, dx_0\right) d\nu \tag{4}$$

Integral with respect to x_0 converges when $\mathrm{Re}[\gamma_h(\nu) - \gamma_r(\omega)] > 0$. This integral is extended to a form that is valid over the entire domain through analytic continuation and evaluated using complex analysis.

2.2 Propagation Constant of Air

When the propagation constant of air is denoted as γ and the propagation distance as r, the sound pressure of a plane wave propagating through air varies according to $e^{-\gamma r}$. The real part of the

propagation constant is specified in the international standard ISO 9613-1 for sound absorption in still air. This model accounts for classical absorption (losses due to viscosity and thermal conduction) and molecular absorption caused by the vibrational relaxation of oxygen and nitrogen molecules in air and is defined as a function of temperature, humidity, atmospheric pressure, and frequency. The imaginary part of the propagation constant can be written as ω/c using the sound speed c, and when frequency dependence exists, the sound speed is treated as $c(\omega)$.

The real and imaginary parts of the propagation constant are related through the Kramers-Kronig relation, based on the requirement that physical responses satisfy causality. Alvarez et al.[8] derived the sound speed from the attenuation constant of ISO 9613-1 using the twice-subtracted Kramers-Kronig relation. In this study, the propagation constant of air was defined using the sound speed function by Alvarez et al. as follows:

$$\gamma(\omega) = \omega^2 \left(\mu_c + \frac{\mu_O}{\omega_O - i\omega} + \frac{\mu_N}{\omega_N - i\omega} \right) - \frac{i\omega}{c_0} \tag{5}$$

where the constants $\mu_c, \mu_O, \mu_N, \omega_O, \omega_N$ are derived from the ISO 9613-1 model, which accounts for environmental factors, including air temperature, humidity, and atmospheric pressure. The constant component of sound speed c_0 vanishes in the integral transformation process in the Kramers-Kronig relation. Therefore, the sound speed at zero frequency by Cramer[9] was employed in this study.

2.3 Exchanging Propagation Constant

Direct calculation of the integral transformation in Equation (4) is impractical because of numerical instability issues[6]. These instabilities primarily arise from the loss of significance (catastrophic cancellation) and amplification of background noise in the numerical integration process. To derive a stable method, this integral was evaluated analytically using complex analysis techniques.

The integral with respect to x_0 in equation (4) is executed under convergent conditions:

$$\int_{-\infty}^{0} \mathrm{e}^{(-\gamma_h(\nu)+\gamma_r(\omega))x_0}\, dx_0 = \frac{1}{-\gamma_h(\nu) + \gamma_r(\omega)} \tag{6}$$

The resulting function is analytic except at poles, so the domain can be extended through analytic continuation. This expression is considered valid regardless of integral convergence. Substituting this into equation (4) and performing the inverse Fourier transform yields the corrected response $r(t)$:

$$r(t) = \frac{1}{2\pi} \int_{-\infty}^{\infty} \frac{d\gamma_h(\nu)}{d\nu} \hat{h}(\nu) \int_{-\infty}^{\infty} \frac{\mathrm{e}^{-i\omega t}}{-\gamma_h(\nu) + \gamma_r(\omega)} d\omega\, d\nu \tag{7}$$

Because $\gamma(\omega)$ is rational in ω and has only four zeros, it is analytic elsewhere in the complex ω-plane, allowing evaluation via residue calculus. Following Jordan's lemma, to ensure causality, the integration path is evaluated along a contour enclosing the lower half-plane. The integral is evaluated as the sum of residues from only the three poles satisfying $\mathrm{Im}\{\omega\} \leq 0$ under the convergence condition $\mathrm{Re}[\gamma_h(\nu) - \gamma_r(\omega)] > 0$. The poles are solutions to:

$$\gamma_r(\omega) = \gamma_h(\nu) \tag{8}$$

Substituting the propagation constant from equation (5) yields a fourth-order equation in ω, which may be addressed using various analytical or numerical solution techniques. The obtained solutions are denoted as $\omega_n^p(\nu),\ n = 1, \cdots, 4$. Under the temperature and humidity conditions numerically confirmed by the authors, one pole position is located at $\mathrm{Im}\{\omega\} > 0$, outside the integration path. The remainder consists of one pole whose imaginary part alternates depending on the sign of $\mathrm{Re}[\gamma_h(\nu) - \gamma_r(\omega)]$, and two poles with consistently negative imaginary parts.

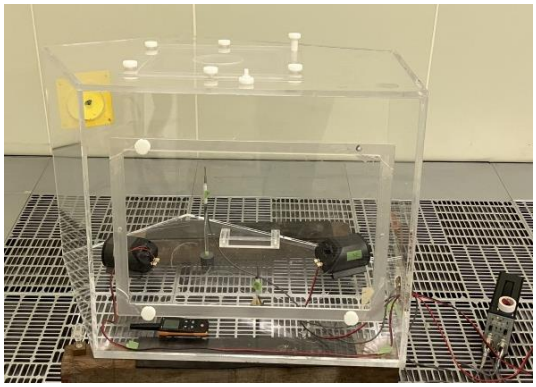

Figure 1. Experimental configuration of the scaled reverberation chamber

	Temperature (°C)	Relative Humidity (%)	Atmospheric Pressure (Pa)
A	15.7	41.0	101,460
B	18.8	53.6	101,480
C	25.1	62.7	101,380
D	29.6	71.1	101,380
E	11.0	39.0	101,480

Table 1. Testing conditions in the scale-model reverberation chamber

Therefore, equation (7) is calculated as

$$r(t) = \int_{-\infty}^{\infty} \frac{d\gamma_h(\nu)}{d\nu} \hat{h}(\nu) \sum_{n=1}^{3} \left(\frac{d\gamma_r\left(\omega_n^p(\nu)\right)}{d\omega} \right)^{-1} e^{-i\omega_n^p(\nu)t}\, d\nu \tag{9}$$

For the dominant pole, the quantity $\left(d\gamma_r\left(\omega_1^p(\nu)\right)/d\omega\right)^{-1}$ is on the order of the speed of sound; by contrast, for the other two poles its magnitude differs by more than 10^{-3}. This dominant pole can be approximated accurately, allowing all residue calculations to be reduced to a single term. A computational formula is derived that uses the measured impulse response $\hat{h}(\nu)$, the propagation constant $\gamma_h(\omega)$ determined from measurement conditions, and the target propagation constant $\gamma_r(\omega)$. As a result, the impulse response amplitude is adjusted by $e^{\mathrm{Im}\{\omega_1^p(\nu)t\}}$, thereby correcting for the effects of air absorption. Here, a stable algorithm has been derived by analytically solving the unstable calculation that completely removes air absorption.

3 EXPERIMENT

3.1 Experimental Setup

To validate the effectiveness of the proposed method, impulse response measurements were conducted using a 1/10 scale empty room acoustic model. The model was constructed from acrylic with a room volume of 0.317 m3 and surface area of 2.82 m2. The experiment was performed under empty room conditions with only the equipment necessary for acoustic measurements-speakers, microphones, various cables, and temperature-humidity sensors-placed inside the model.

The experiment was conducted in a controlled environmental chamber capable of regulating temperature from 5°C to 40°C and relative humidity from 30% to 80%. Temperature and humidity measurements were performed using a testo 625 hygrometer, while atmospheric pressure was measured using a testo 511 barometer. After each environmental change, approximately 30 minutes were allowed for air stabilization inside the model, with the model openings remaining open during this period. During the measurements, the openings were sealed with acrylic covers. Atmospheric pressure was measured outside the model as it remained constant throughout the laboratory.

A ribbon tweeter (Pioneer PT-R4) was used as the sound source. A 1/8-inch condenser microphone (B&K 4138) was employed for sound reception. Signal input and output were handled by an AD/DA

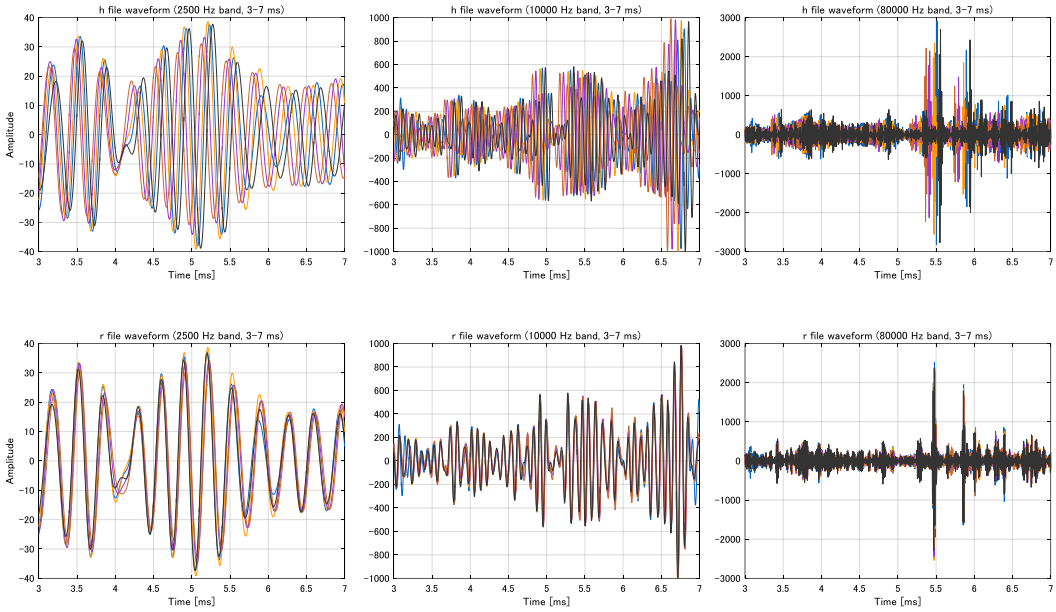

Figure 2. Octave band (2,500Hz, 10,000Hz, 80,000Hz) impulse response waveforms (3-7msec): measured (top row) and corrected for Condition B 18.8°C, 53.6%, 101,480Pa (bottom row)

converter (NI PXIe-6386) with a sampling frequency set to 1 MHz. A 60-second time stretched pulse was used as the measurement signal, with no synchronous averaging performed.

3.2 Experimental Result of Propagation Constant Correction

In this study, we first converted all impulse responses (conditions A, C–E) to a common reference (condition B) using our proposed method. However, when the correction formula (9) is applied directly, the background noise signals change exponentially—either amplifying or decaying—which distorts late-time responses. To stabilize the background noise levels, we introduce an amplitude correction factor $G(\nu, t)$

$$e^{-i\omega_1^p(\nu)t} \longmapsto e^{-i\mathrm{Re}\{\omega_1^p(\nu)\}t} G(\nu, t), \qquad G(\nu, t) = \frac{e^{-(\delta_0/N+\delta)\mathrm{t}} + (b/a)^{1+N\delta/\delta_0}}{e^{-\delta_0 t/N} + b/a} \tag{10}$$

where $\delta = -\mathrm{Im}\{\omega_1^p(\nu)\}$, and a, b, δ_0 are values obtained through parameter fitting, assuming that the amplitude of the measured impulse response can be expressed as $a\, e^{-\delta_0 t} + b$ for frequency ν. The values of a, b, δ_0 obtained for 1/3-octave band signals were extended to continuous frequency ν through interpolation. This amplitude correction function preserves the crossover time $t_M = {\delta_0}^{-1}\log(a/b)$, where $a\, e^{-\delta_0 t_M} = b$. The time t_M separates the signal domain from the noise floor, with the signal level at the crossover time being $a\, e^{-(\delta_0+\delta)t_M}$ at the crossover time. The corrected impulse response $r(t)$ also maintains the temporal structure of $a\, e^{-\delta_0 t} + b$. This corresponds to the noise scaling concept proposed by Ćirić et al.[4].

Figure 2 shows the initial impulse responses of measured and corrected values. While differences in amplitude and phase due to temperature and humidity variations were observed in the uncorrected impulse responses, the corrected responses showed good agreement in both phase and amplitude. In the 80,000 Hz band, wave packet alignment was observed, although some phase discrepancies remained. Such errors may be attributed to measurement errors in air temperature and humidity and modeling errors in the propagation constant, among other factors, although the details remain unclear.

The reverberation times T20 obtained from Schroeder integration of the impulse responses are shown

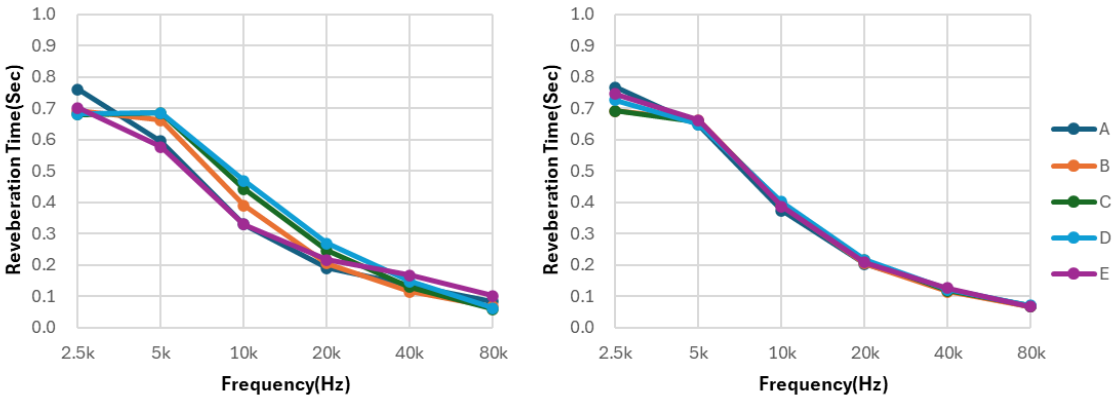

Figure 3. Reverberation times for octave band signals
(left) before correction; (right) after correction

in Figure 3. The scatter in the data observed among conditions in the uncorrected signals was significantly reduced through application of the proposed method, showing good agreement. The slight remaining scatter in the 2,500 Hz band is attributed to an insufficient signal-to-noise ratio due to the low signal amplitude.

3.3 Experimental Result of Scale Conversion

The reverberation model was treated as a 1/10 scale reverberation room model, and the impulse response was converted to full-scale conditions. The propagation constant determined from the air conditions was reduced to 1/10 of the measured value according to Equation (3), and the correction formula was calculated. The target correction conditions were set to 20°C, 50%, and 101,315 Pa atmospheric pressure.

The initial waveforms are shown in Figure 4. Similar to Figure 4 (lower panel) where air conditions were modified, results showing wave packet alignment were obtained. The band-wise level waveforms of the full-scale impulse responses are shown in Figure 5 (condition E) and Figure 6 (condition D). For comparison, the measured values before applying scale transformation and correction were plotted with the time scale expanded by a factor of 10. Attenuation is corrected and signal amplification is confirmed. The noise floor increases, and the signal-to-noise ratio (SNR) decreases in certain bands (e.g., 8 kHz for condition D).

The reverberation time RT20 after scale transformation and propagation constant correction is shown in Figure 7. Even with correction including scale transformation, the corrected reverberation times show good agreement. However, for conditions C and D at 8 kHz band, the reverberation time could not be determined owing to the increased background noise.

The experimental results demonstrate that the proposed analytical method successfully corrects both amplitude characteristics (absorption) and waveform properties (dispersion) while simultaneously handling scale transformation and temperature-humidity condition corrections. The method maintained high accuracy across different environmental conditions and scale factors, validating its effectiveness for practical-scale model applications in architectural acoustics.

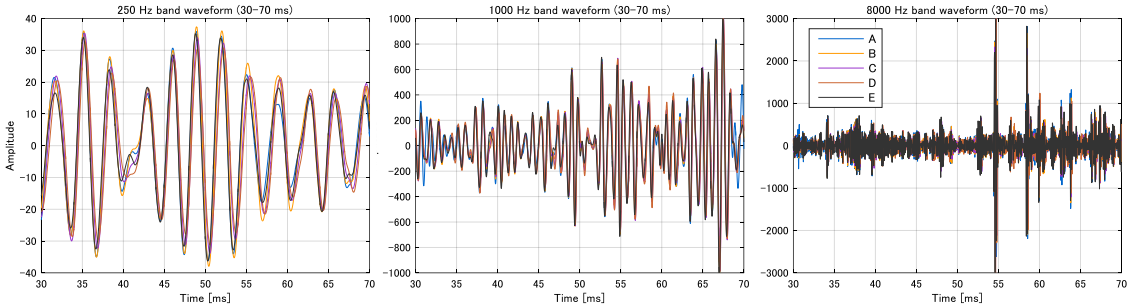

Figure 4. Corrected impulse responses for scale-model measurements under Conditions A-E, converted to full scale by a factor of 10. From left to right: octave-band signals at 2 500 Hz, 10 000 Hz, and 80 000 Hz

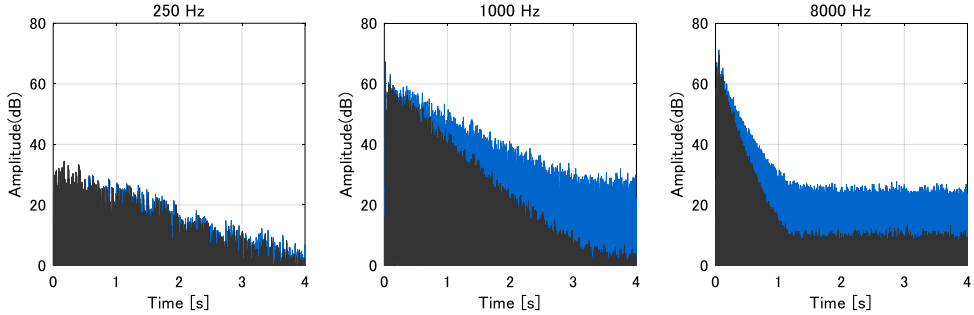

Figure 5. impulse responses measured under Condition E in three frequency bands (250Hz, 1000Hz, 8000Hz). black: measured response with time axis stretched tenfold, blue: responses after applying a scale and propagation constant conversion

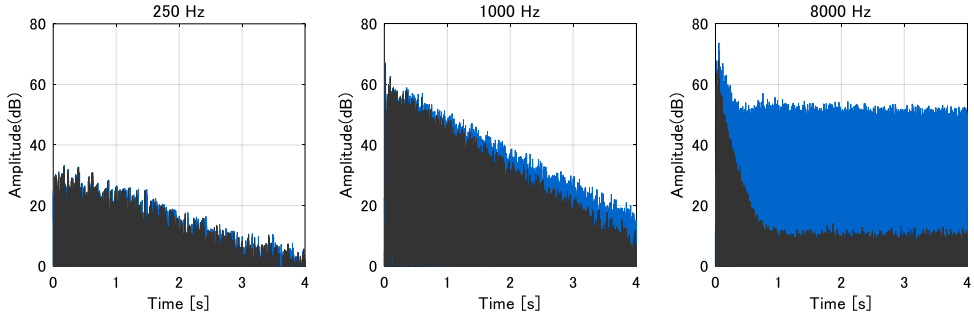

Figure 6. impulse responses measured under Condition D in three frequency bands (250Hz, 1000Hz, 8000Hz). black: measured response with time axis stretched tenfold, blue: responses after applying a scale and propagation constant conversion

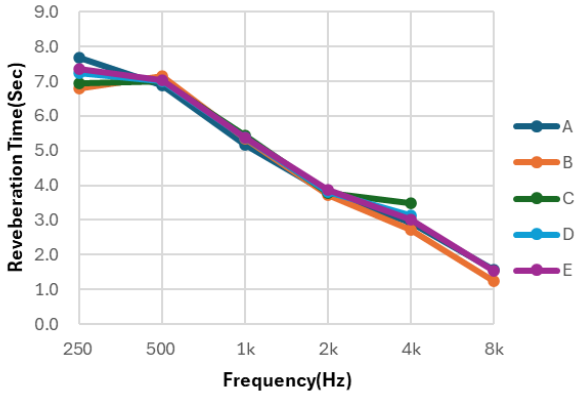

Figure 7 Reverberation time RT20 of impulse responses after transformation (8k bands for conditions C and D omitted due to low SNR)

4 CONCLUSION

This study presents an analytical framework for correcting air absorption and dispersion in acoustic scale model experiments. By treating the problem in the complex-analytic domain, the method unifies impulse responses measured under varying atmospheric and scale conditions. The proposed framework demonstrates precise alignment of waveforms, correcting discrepancies in both phase and amplitude.

To manage the noise amplification inherent in this process, an amplitude correction function was implemented to stabilize the background noise floor. This function managed noise under most conditions, preserving the signal's temporal structure while preventing exponential noise growth. However, in cases involving low initial signal-to-noise ratio (SNR) and large required absorption correction, residual noise impeded the reliable determination of parameters such as reverberation time. This demonstrates that the quality of the corrected signal depends on that of the initial measurement.

5 REFERENCES

1. Barron, M. "Auditorium Acoustic Modeling Now." Applied Acoustics 16 (4): 279-90 (1983).
2. J. D. Polack, A. H. Marshall, and G. Dodd, "Digital evaluation of the acoustics of small models: The MIDAS package," J. Acoust. Soc. Am. 85, 185-193 (1989).
3. H. A. Akil, D. J. Oldham, and B. M. G. Cheetham, "Digital correction for excessive air absorption in acoustic scale models," Proc. Inst. Acoust. 16(2), 525-532 (1994).
4. D. G. Ćirić and A. Pantić, "Numerical Compensation of Air Absorption of Sound in Scale Model Measurements," Arch. Acoust. 37(2), 219-225 (2012).
5. K. Suzuki, S. Koyanagi, and T. Hidaka. “Auralization of Three-Dimensional Sound Field in an Acoustic Scale Model Using Laser-Induced Sound Sources.” In 2023 Immersive and 3D Audio: From Architecture to Automotive (I3DA), 1–7. IEEE.
6. S. Koyanagi et al., "Proposal of air absorption and dispersion correction method for impulse response," (2013), "Evaluation of air-absorption and dispersion correction method for impulse response," (2016), "A comparison of air-absorption correction method for impulse response," (2017), Proc. Autumn Meet. Acoust. Soc. Jpn. in Japanese.
7. S. Koyanagi et al., "Analytical approach to air absorption and dispersion correction for impulse response,", Proc. Autumn Meet. Acoust. Soc. Jpn. (2024) in Japanese.
8. F. J. Álvarez and R. Kuc, "Dispersion relation for air via Kramers-Kronig analysis," J. Acoust. Soc. Am. 124, EL57-EL61 (2008)
9. O. Cramer, "The variation of the specific heat ratio and the speed of sound in air with temperature, pressure, humidity, and CO2 concentration," J. Acoust. Soc. Am. 93, 2510-2516 (1993).